Eur. J. Mineral.
2019, **31**, 465–471
Published online 10 January 2019

Segelerite from the Mount Deverell variscite deposit, Western Australia. Hydrogen bonding and relationship to jahnsite

Ian E. GREY[1,*], W. Gus MUMME[1], Peter J. DOWNES[2], Benjamin A. GRGURIC[3] and Robert W. GABLE[4]

[1]CSIRO Mineral Resources, Private Bag 10, Clayton South, Victoria 3169, Australia
*Corresponding author, e-mail: ian.grey@csiro.au
[2]Earth and Planetary Sciences, Western Australian Museum, Locked Bag 49, Welshpool DC, Western Australia 6986, Australia
[3]Centre for Exploration Targeting, University of Western Australia, 35 Stirling Highway, Crawley, Western Australia 6009, Australia
[4]School of Chemistry, University of Melbourne, Parkville, Victoria 3010, Australia

Abstract: The crystal structure of segelerite, $Ca_2Mg_2Fe^{3+}_{1.4}Al_{0.6}(PO_4)_4(OH)_2(H_2O)_8$, from the Mount Deverell variscite deposit, Western Australia, has been refined using single-crystal X-ray data to $wR_{obs} = 0.048$ for 2082 unique reflections and all H atoms were located during the refinement. Cell parameters are $a = 14.7772(2)$ Å, $b = 18.7079(2)$ Å, $c = 7.2424(1)$ Å, space group *Pbca*. The H-bonding scheme is described and compared to that for the combinatorial polymorph, jahnsite. The crystal structures of both minerals comprise heteropolyhedral slabs of composition $[XM1Fe^{3+}_2(OH)_2(PO_4)_4]$, that are linked together *via* corner-sharing of PO_4 tetrahedra with isolated $[M2(O_p)_2(H_2O)_4]$ octahedra. The structures differ in the mode of linkage of the *M*2 octahedra, which is *via trans* O_p ligands in segelerite and *via* both *trans* and *cis* O_p ligands in jahnsite. In segelerite, $X = M1 = Ca$, whereas in jahnsite-group minerals, $X = Ca$, Na, Mn^{2+} and $M1 = Mn^{2+}$, Mg^{2+}, Fe^{2+}, Fe^{3+}. *X* and *M*1 alternate along the 7 Å axis and it is proposed that different magnitudes of rotation of the Fe^{3+} octahedra about the 7 Å axis to accommodate the different coordination requirements of the *X* and *M*1 cations drives the symmetry changes in the two minerals so that a strong H-bonding network is maintained.

Key-words: segelerite; jahnsite; H-bonding; crystal structure; single-crystal refinement; combinatorial polymorphs.

1. Introduction

The Mt. Deverell and Mt. Deverell East variscite deposits, located 15 km north-northwest of Milgun Station in the central western Gascoyne region of Western Australia, are important as the main source of gemstone variscite production in Western Australia (850 *t* produced from opencut mines between 1992 and 2005). The deposits host a wide range of secondary phosphate minerals, including collinsite, turquoise, gordonite, foggite, crandallite, wardite, hydroxylapatite, leucophosphite, mitridatite, montgomeryite, and rockbridgeite (Bridge & Pryce, 1974; Fetherston *et al*., 2013).

In a recent study on the secondary phosphate minerals from Mt. Deverell, some hand specimens were found to contain clusters of pale-olive rod-like crystals up to 2 mm long encrusting cavities, shown in Fig. 1. Initial powder X-ray diffraction (XRD) identification coupled with energy-dispersive spectroscopy (EDS) suggested that they were a jahnsite-group species containing Ca, Mg and Fe, but subsequent single-crystal studies confirmed them as segelerite. Both segelerite and jahnsite were characterised as new species by Moore (1974). Moore & Araki (1974) solved the crystal structure of jahnsite-(CaMnMg) and they subsequently reported the crystal structure for segelerite (Moore & Araki, 1977). They noted the similarity of the crystal-chemistry of the two minerals: both have structures based on dense heteropolyhedral slabs of composition $[XM1Fe^{3+}_2(OH)_2(PO_4)_4]$,that are linked together *via* corner-sharing of PO_4 tetrahedra with isolated $[M2(O_p)_2(H_2O)_4]$ octahedra. In segelerite, $X = M1 = Ca$, whereas in jahnsite-group minerals, $X = Ca$, Na, Mn^{2+} and *M*1 and $M2 = Mn^{2+}$, Mg^{2+}, Fe^{2+}, Fe^{3+}. The structures differ in the mode of linkage of the *M*2 octahedra, which is *via trans* O_p ligands in segelerite and *via* both *trans* and *cis* O_p ligands in jahnsite. The different isomeric arrangements are associated with a change in symmetry from orthorhombic, *Pbca* with $a \sim 14.8$, $b \sim 18.7$, $c \sim 7.3$ Å for segelerite to monoclinic, *P*2/*a*, with $a \sim 14.9$, $b \sim 7.1$, $c \sim 9.9$ Å, $\beta \sim 110.2°$ for jahnsite, where $a_{seg} \sim a_J$, $b_{seg} \sim 0.5\ a_J + 2\ c_J$ and $c_{seg} \sim b_J$. The two structures are shown in projection along their 7 Å axes in Fig. 2.

Moore & Araki (1977) described the two minerals as combinatorial polymorphs with structural formulae expressed in the form:

0935-1221/19/0031-2829 $ 3.15
https://doi.org/10.1127/ejm/2019/0031-2829

Fig. 1. Segelerite crystals from Mount Deverell, with attached small spheres of hydroxylapatite crystals. Field of view 6.4 mm.

$$\text{Segelerite}: \left[Mg(H_2O)_4\right]_2\left[Ca_2Fe_2^{3+}(OH)_2(PO_4)_4\right]$$
$$\text{Jahnsite-CaMnMg}: \left[Mg(H_2O)_4\right]_2\left[CaMnFe_2^{3+}(OH)_2(PO_4)_4\right]$$

The authors emphasised the importance of exploring the structural differences between the two structure types, because "combinatorial isomerism is one of the underlying principles which govern the great species diversity among low-temperature oxysalts". A significant contributor to the relative stability of the two isomeric forms would be expected to be the H-bonding topology (Herwig & Hawthorne, 2006; Gatta *et al.*, 2014). Direct location of H atoms from high-quality single-crystal structure refinements has been reported for a number of jahnsite-group minerals (Kampf *et al.*, 2008; Capitelli *et al.*, 2011; Kampf *et al.*, 2016) but the equivalent information for segelerite is lacking. The only published refinement for segelerite is that by Moore & Araki (1977) but owing to the low diffracting quality of the available type-specimen crystals, the reliability factor was very high (R = 28%) and the authors could not directly locate the H atoms during the refinement. Nevertheless they proposed a H-bonding scheme based on geometric and steric considerations.

Segelerite crystals from Mt. Deverell proved to be of good diffracting quality and we were able to locate all H atoms directly from difference-Fourier maps during the crystal-structure refinement. We report here our crystallographic study of segelerite from Mt. Deverell and a comparison of the crystal chemistry of segelerite and jahnsite.

2. Specimen occurrence and mineralogy

The host rocks at Mt. Deverell (latitude −24.99096; longitude 118.20305) are marine sedimentary rocks of the Mesoproterozoic Edmund Basin situated within the Capricorn Orogen. Variscite and metavariscite occur in narrow veins that crosscut silicified shale and mudstone (Fetherston *et al.*, 2013). Secondary phosphate minerals have replaced variscite veins in the oxidized zone at Mt. Deverell, where the phosphate was likely derived from the dissolution of apatite in low-pH groundwaters. The crystals of segelerite analysed in this study were sampled from a specimen collected from loose material near the exposed face of the quarry (specimen number WAM M70.2014). Segelerite encrusts a small cavity, ~8 mm long, in oxidised siltstone that contains quartz veining and abundant massive to botryoidal goethite–hematite. Segelerite is overgrown by spheres of radiating hydroxylapatite crystals (Fig. 1) and is restricted to one cavity in the specimen. Associated cavities, to 15 mm long, contain a thin crust of leucophosphite coated with mitridatite that is overgrown by crystals of collinsite (up to 2 mm long) and then two generations of hydroxylapatite comprising prisms (less than 1 mm long) and radiating spheres.

3. Experimental procedure

3.1. Analyses

Electron microprobe (EMP) analyses were done using wavelength-dispersive spectrometry on a JEOL JXA 8500F Hyperprobe operated at an accelerating voltage of 15 kV and a beam current of 5 nA. The beam was defocused to 5 μm for the analyses, but some beam damage was still evident, and low analysis totals were obtained. Average of 16 analyses on a compositionally zoned (Fe/Al) crystal gave CaO 13.8, MgO 10.3, Fe_2O_3 13.6, Al_2O_3 3.77, P_2O_5 33.6 wt%. The Fe_2O_3/Al_2O_3 zoning varied linearly (R^2 = 0.97) between 9.0/7.6 and 18.0/0.8 wt% oxides. The empirical formula scaled to 4 PO_4 and charge-balanced with OH is $Ca_{2.06}Mg_{2.18}(Fe_{1.43}Al_{0.62})(PO_4)_4(OH)_{2.63}(H_2O)_8$. The simplified formula is $Ca_2Mg_2(Fe_{1.4}Al_{0.6})(PO_4)_4(OH)_2(H_2O)_8$.

3.2. Crystallography

Single-crystal diffraction data were collected using a Rigaku XtaLAB Synergy diffractometer at the School of Chemistry, University of Melbourne. Data were collected to a resolution of 0.79 Å at 293 K using a HyPix CCD Plate detector and Cu$K\alpha$ radiation.

A structure solution for all non-H atoms in space group *Pbca* was obtained using SHELXT (Sheldrick, 2015), which was consistent with the structural model for segelerite reported by Moore & Araki (1977). The structure was refined using JANA2006 (Petříček *et al.*, 2014). In the course of the refinement, all H atoms were located in difference-Fourier maps. Their coordinates were refined with the restraints O−H = 0.85(1) Å and H–O–H = 109.47(1) for the H atoms associated with water molecules. A common isotropic displacement parameter was refined for the H atoms, while all other atoms were refined anisotropically. Refinement of the site occupancy for the Fe site gave only 0.85 occupancy. Al was located with the Fe in this site and their site occupancies were refined subject to the constraint of full occupancy by Fe + Al. The refinement converged to wR_{obs} = 0.048 for 2082 unique reflections. Further details

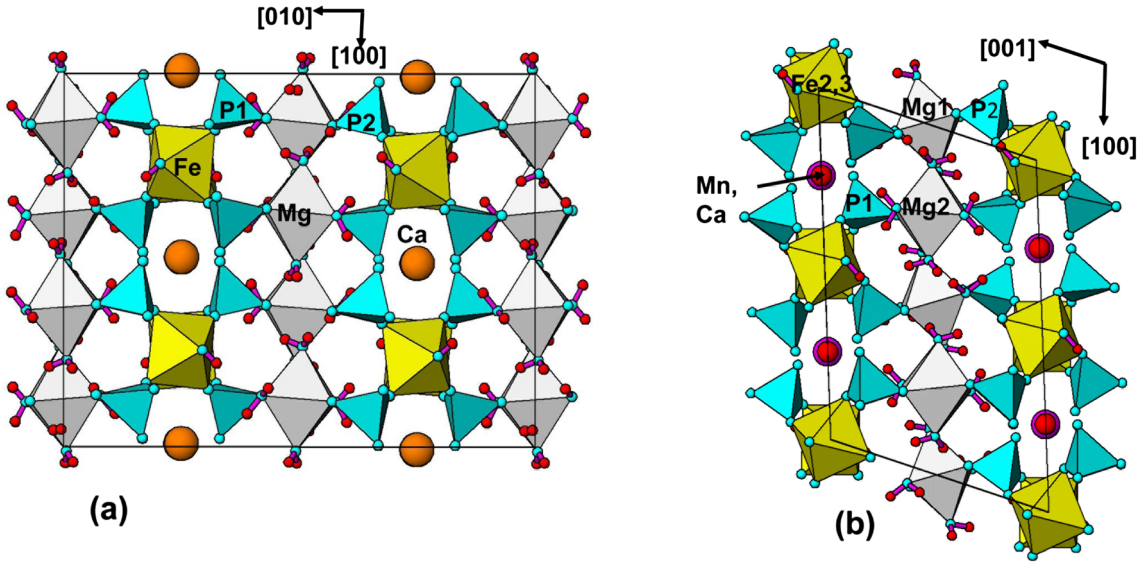

Fig. 2. Projection along the 7 Å axis of structures of (a) segelerite and (b) jahnsite (H atoms from Kampf *et al*., 2008).

of the data collection and refinement are given in Table 1. Refined coordinates and equivalent isotropic-displacement parameters (Å^2), plus bond-valence sums (BVS) (Gagné & Hawthorne, 2015) are reported in Table 2 and polyhedral bond distances are given in Table 3. Note that the phosphate anions O1–O8 are ordered differently to reported by Moore & Araki (1977), so that they are consistent with the labelling used for jahnsite-(NaFeMg) by Kampf *et al*. (2008), allowing direct comparison of the bonding in the two minerals. Thus O1 and O5 are non-bridging phosphate anions, O2 and O6 corner-link to Mg octahedra and O3, O4, O7 and O8 corner-link to Fe octahedra (Table 3).

Table 1. Data collection and refinement conditions for segelerite.

Formula	$Ca_2Mg_2Fe^{3+}_{1.4}Al_{0.6}(PO_4)_4(OH)_2(H_2O)_8$
Molecular weight	781.9
Temperature	293 K
Wavelength	1.5418 Å
Crystal system/space group	Orthorhombic *Pbca*
Unit-cell dimensions	a = 14.7772(2) Å b = 18.7079(2) Å c = 7.2424(1) Å
Cell volume, Z	V = 2002.16(4) Å^3, Z = 4
Density (calc.)	2.59 g cm^{-3}
Absorption coefficient	18.09 cm^{-1}
Crystal size	0.09 × 0.11 × 0.47 mm^3
Data collection, θ range	4.73–77.9°
Reflections collected	24 744
Unique reflections, R_{int}	2082, 0.093
Observed reflections, $I > 3\sigma(I)$	1759
Data coverage	99%
Parameters/restraints/constraints	192/13/17
R indices, observed reflections	R_{obs} = 0.039, wR_{obs} = 0.046
R indices, all data	R_{obs} = 0.046, wR_{obs} = 0.048
Largest difference peak and hole	+0.56 and −0.65 e Å^{-3}

4. Discussion

The structural model for segelerite confirms the original model of Moore & Araki (1977). From the refined Al/Fe occupancies in the Fe site the formula for the Mt. Deverell segelerite is $Ca_2Mg_2Fe^{3+}_{1.43}Al_{0.57}(PO_4)_4(OH)_2(H_2O)_8$, corresponding to a solid solution of dominant segelerite with minor overite, $Ca_2Mg_2Al_2(PO_4)_4(OH)_2(H_2O)_8$ (Larsen, 1940). The Al-content from the site-occupancy refinement is consistent with the BVS for the Fe site (Table 2) and agrees with the mean Fe/Al atomic ratio obtained from the EMP analyses.

4.1. H-bonding in segelerite and jahnsite

The H-bonding scheme for segelerite from this study is reported in Table 4. There is some agreement with the scheme proposed by Moore & Araki (1977). These authors, however, considered only phosphate anions as acceptors and proposed that the hydroxyl group was not involved in H-bonding, whereas the results in Table 4 show that the hydroxyl, Oh, and three of the four H_2O are involved as both donors and acceptors. For jahnsite we will refer to the H-bonding scheme for jahnsite-(NaFeMg) reported by Kampf *et al*. (2008). Their scheme has been verified in recent studies of other jahnsite-group minerals (Capitelli *et al*., 2011; Kampf *et al*., 2016). For both minerals, the H-bonding is dominated by the contributions of the four Mg-coordinated H_2O molecules, Ow1–Ow4. As shown in Fig. 2 the Mg octahedra lie in planes parallel to the heteropolyhedral slabs, (010) in segelerite and (001) in jahnsite. For ease of visualisation we will refer to Ow3 and Ow4 that have Ow–Mg oriented along [100] in Fig. 2 as apical H_2O, and Ow1 and Ow2, lying in the plane normal to [100], as equatorial H_2O. This plane contains also the O_p anions O2 and O6 that corner-link the Mg octahedra to PO_4 groups. In the segelerite crystal structure, the Mg atoms

Table 2. Refined coordinates and equivalent isotropic-displacement parameters (Å^2), plus bond-valence sums (BVS) for segelerite.

	SOF	*x*	*y*	*z*	U_{iso}	BVS (*vu*)*
Fe	0.716(5) Fe + 0.284 Al	0.25858(3)	0.25060(2)	0.24793(7)	0.0158(2)	3.04
Ca	1	0.00764(4)	0.24925(3)	0.24213(6)	0.0231(2)	2.04
P1	1	0.39429(4)	0.34981(3)	0.49379(9)	0.0170(2)	5.03
P2	1	0.12295(4)	0.35065(3)	0.50590(9)	0.0168(2)	4.99
Mg	1	0.12703(5)	0.50103(5)	0.7522(1)	0.0189(3)	2.06
O1	1	0.4963(1)	0.33148(9)	0.5096(2)	0.0219(5)	1.84 (2.04)
O2	1	0.3794(1)	0.4295(1)	0.4742(3)	0.0244(6)	1.67 (2.07)
O3	1	0.3493(1)	0.3206(1)	0.6677(3)	0.0278(5)	1.92
O4	1	0.3634(1)	0.30817(9)	0.3210(2)	0.0217(5)	2.04
O5	1	0.0215(1)	0.33177(9)	0.4868(3)	0.0225(5)	1.85 (2.05)
O6	1	0.1375(1)	0.43034(9)	0.5333(3)	0.0227(5)	1.65 (1.95)
O7	1	0.1530(1)	0.30752(9)	0.6773(2)	0.0214(5)	2.01
O8	1	0.1696(1)	0.32441(9)	0.3294(3)	0.0258(5)	1.85
Oh	1	0.2573(1)	0.2955(1)	−0.0024(3)	0.0205(5)	0.97 (1.97)
Ow1	1	0.1186(1)	0.5792(1)	0.5451(3)	0.0259(6)	0.33 (2.03)
Ow2	1	0.1358(1)	0.4214(1)	0.9573(3)	0.0248(5)	0.32 (2.12)
Ow3	1	−0.0128(1)	0.4939(1)	0.7512(3)	0.0305(6)	0.35 (1.95)
Ow4	1	0.2675(1)	0.5076(1)	0.7510(3)	0.0257(6)	0.34 (2.14)
Hoh	1	0.220(3)	0.329(2)	−0.015(5)	0.052(4)	
Hw1a	1	0.068(2)	0.599(2)	0.531(5)	0.052(4)	
Hw1b	1	0.159(2)	0.609(1)	0.543(6)	0.052(4)	
Hw2a	1	0.090(2)	0.395(2)	0.976(4)	0.052(4)	
Hw2b	1	0.156(2)	0.435(2)	1.057(4)	0.052(4)	
Hw3a	1	−0.043(2)	0.479(2)	0.843(3)	0.052(4)	
Hw3b	1	−0.046(2)	0.493(2)	0.656(3)	0.052(4)	
Hw4a	1	0.295(2)	0.523(2)	0.845(4)	0.052(4)	
Hw4b	1	0.294(2)	0.470(2)	0.712(5)	0.052(4)	

**Note*: Numbers in parentheses include H-contributions of 0.8 (donor), 0.2 (acceptor) and 0.1 (bifurcated acceptors).

Table 3. Polyhedral bond-distances (Å) in segelerite.

Fe–O3	1.977(2)	Ca–O1	2.354(2)
Fe–O4	1.960(2)	Ca–O1	2.391(2)
Fe–O7	1.969(2)	Ca–O3	2.759(2)
Fe–O8	1.996(2)	Ca–O4	2.442(2)
Fe–Oh	1.999(2)	Ca–O5	2.359(2)
Fe–Oh	2.003(2)	Ca–O5	2.400(2)
Av.	1.984	Ca–O7	2.442(2)
		Ca–O8	2.846(2)
P1–O1	1.551(2)	Av.	2.500
P1–O2	1.513(2)		
P1–O3	1.525(2)		
P1–O4	1.543(2)	Mg–O2	2.070(2)
Av.	1.533	Mg–O6	2.070(2)
		Mg–Ow1	2.099(2)
P2–O5	1.546(2)	Mg–Ow2	2.108(2)
P2–O6	1.519(2)	Mg–Ow3	2.070(2)
P2–O7	1.546(2)	Mg–Ow4	2.080(2)
P2–O8	1.533(2)	Av.	2.083
Av.	1.536		

are in general positions and so the octahedra have the composition $Mg(O_p)_2Ow1Ow2Ow3Ow4$, whereas in jahnsite there are two independent Mg sites, Mg1 and Mg2, with site symmetry −1 and 2, respectively. The Mg1 octahedron has the composition $Mg(O_p)_2(Ow3)_2(Ow2)_2$, with all pairs of ligands in *trans* configuration, while the Mg2 octahedron has the composition $Mg(O_p)_2(Ow4)_2(Ow1)_2$, with *cis* O_p and Ow1 ligands and *trans* Ow4 ligands.

In Fig. 3 the H-bonding in the layers of Mg octahedra are compared for the two minerals. In segelerite (Fig. 3a) the majority of the H-bonds (6 out of 10) lie within the plane of octahedra. The apical Ow3 and Ow4 each H-bond to both O2 and O6 in adjacent Mg octahedra, and so these anions each receive two H-bonds. The apical Ow3 is involved in a bifurcated bond to O6 and Ow1. In contrast, the equatorial Ow1 and Ow2 are involved in predominantly out-of-plane H-bonds. Ow1 is a donor to Oh and to the non-bridging phosphate anion O5, and Ow2 is a donor to a non-phosphate anion O1. Only the bond of Ow2 to the apical Ow4 of an adjacent Mg octahedron is an in-plane bond. In Table 2, the BVS values for the anions involved in H-bonding have the H contributions included in the numbers given in parentheses and these are close to two in all cases. In jahnsite (Fig. 3b) only a minority of the H bonds (4 out of 9) lie in the plane of the Mg octahedra. The apical Ow3 and Ow4 have only one H-bond each to the equatorial O_p anions, O2 and O6, respectively, compared with two such bonds in segelerite. The second H-bond from Ow3 is to the equatorial Ow1 in an adjacent octahedron, and the second Ow4 bond is to a phosphate anion, O8, that corner-connects to an Fe octahedron. The equatorial Ow1 and Ow2 molecules H-bond to the same acceptors as in segelerite, *i.e.* Ow1 donates to Oh and the non-bridging anion O5 while Ow2 donates to the apical Ow4 and the second non-bridging phosphate anion O1. For both minerals, bonds to

Table 4. Hydrogen bonds in segelerite.

Donor	H	Acceptor	D–H (Å)	H...A (Å)	D–A (Å)	A–H...D (°)
Oh	HOh	Ow2	0.84(4)	2.14(4)	2.975(3)	174(4)
Ow1	Hw1a	O5	0.85(3)	1.85(3)	2.668(3)	162(3)
Ow1	Hw1b	Oh	0.82(3)	2.19(3)	2.995(3)	166(3)
Ow2	Hw2a	O1	0.85(4)	1.82(4)	2.670(3)	173(3)
Ow2	Hw2b	Ow4	0.82(3)	2.10(3)	2.887(3)	160(3)
Ow3	Hw3a	O2	0.84(3)	1.99(3)	2.819(3)	168(3)
Ow3	Hw3b	O6	0.84(3)	2.40(3)	3.107(3)	142(3)
Ow3	Hw3b	Ow1	0.84(3)	2.27(3)	2.988(3)	144(4)
Ow4	Hw4a	O6	0.84(3)	1.91(3)	2.739(3)	171(3)
Ow4	Hw4b	O2	0.85(3)	2.27(3)	2.981(3)	142(3)

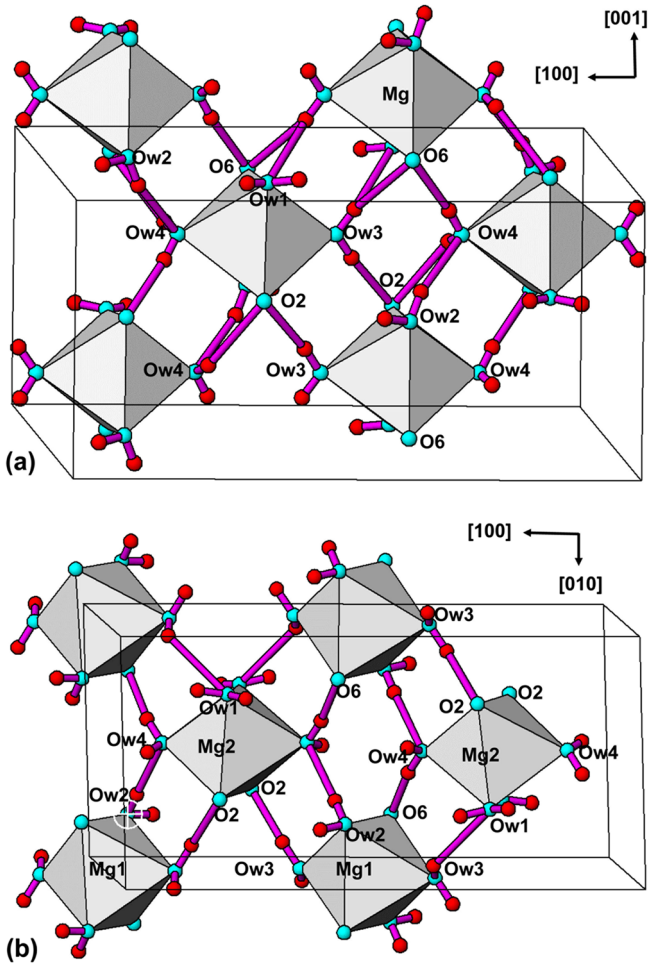

Fig. 3. H-bonding within (a) the (010) layer of Mg octahedra in segelerite, (b) the (001) plane of Mg octahedra in jahnsite.

the non-bridging phosphate anions, O1 and O5, and to the equatorial anions, O2 and O6, are the strongest of the H-bonds with O–O < 2.86 Å.

4.2. Heteropolyhedral layers in segelerite and jahnsite

An interesting topological distinction between the structures of segelerite and jahnsite concerns the way that the 7 Å columns, $Fe_2^{3+}(OH)_2(PO_4)_4$, connect to one another *via* the Mg octahedra. In segelerite the columns and the intervening pairs of Mg octahedra form bands parallel to (100) shown in Fig. 4. The bands have composition $[Fe_2(PO_4)_4(OH)_2Mg_2(H_2O)_8]^{4-}$ which are charge-balanced by $2Ca^{2+}$. Adjacent bands are held together only by relatively weak Ca–O bonds, together with H-bonding. In Fig. 4, adjacent bands have been separated to illustrate this feature, by which segelerite can be described as a layer structure with interlayer Ca. The strongest H-bonds in segelerite, from the equatorial Ow1 and Ow2 to the non-bridging phosphate anions O5 and O1, occur across the interlayer region and reinforce the interlayer Ca–O bonding. In jahnsite the (100) planes of corner-connected $Fe_2^{3+}(OH)_2(PO_4)_4$ and $Mg(H_2O)_4$ have the composition $[Fe_2(PO_4)_2(OH)_2Mg(H_2O)_4]$ and they are separated by planes of composition $[XM1(PO_4)_2Mg(H_2O)_4]$. The two types of planes are interconnected *via* bonds from PO_4 in the *XM*1... layer to the Fe octahedra in the adjacent planes on either side. Thus jahnsite cannot be described as a simple layer structure in the same way as segelerite. The situation in the jahnsite structure is further complicated by the presence of a pseudo-mirror plane normal to [100], resulting in bifurcation of the $[Fe_2(PO_4)_2(OH)_2Mg(H_2O)_4]$ planes parallel to (100) and $(20\bar{1})$ as shown in Fig. 5. The bifurcation of the two planes gives a cross-hatched pattern of planes with *X* and *M*1 cations contained within diamond-shaped channels.

4.3. Role of octahedron rotations in determining structure type

An important distinction between the crystal-chemistry of segelerite and jahnsite is that segelerite contains 7 Å chains of cations of one type (Ca^{2+}) located between the $Fe_2^{3+}(OH)_2(PO_4)_4$ columns, whereas jahnsite-group minerals, with general formula $XM1M2_2M3_2(PO_4)_4(OH)_2(H_2O)_8$ (Kampf *et al.*, 2016, 2019) have alternating large *X* (Ca^{2+}, Na^+) and small *M*1 (Mg^{2+}, Fe^{2+}, Mn^{2+}, Fe^{3+}) cations in the 7 Å chains. As shown in Fig. 6, the cation coordination environment involves four non-bridging phosphate anions (2 × O1 + 2 × O5) and two octahedron edges (anions O3, O4, O7, O8 in Fig. 6). In segelerite the four Ca–O1 and Ca–O5 distances are 2.35–2.40 Å. Small (~5°) rotations of the Fe octahedra about the 7 Å axis bring one vertex of each octahedral edge (O4 and O7) to similar distances from the Ca (Ca–O4 and Ca–O7 = 2.44 Å) while elongating the distances

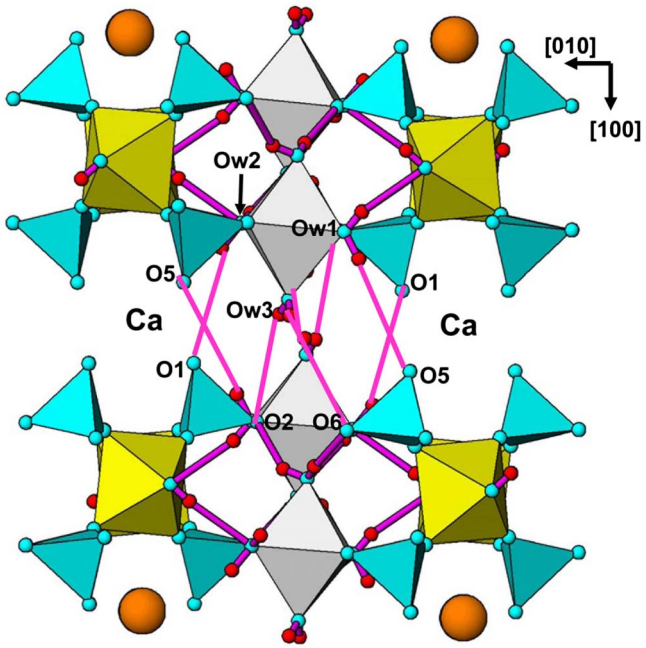

Fig. 4. Heteropolyhedral layers parallel to (100) in segelerite. Adjacent layers have been separated to emphasise the interlayer H-bonding.

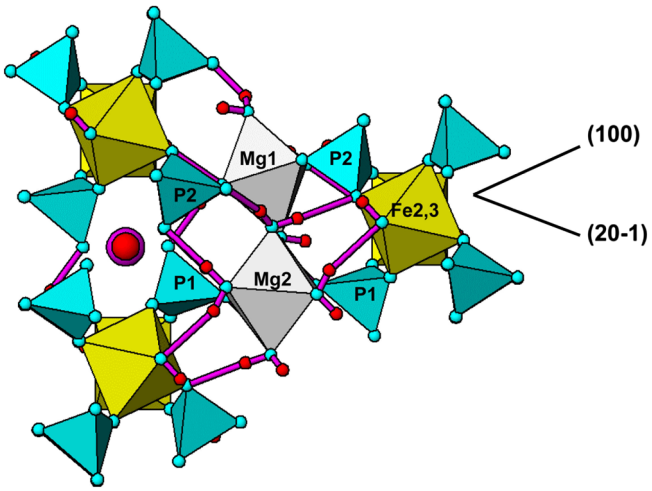

Fig. 5. A projection along the 7 Å axis of part of the jahnsite structure, showing the pseudo-twinning between the (100) and (20$\bar{1}$) planes.

to the other vertices (Ca–O3 = 2.76, Ca–O8 = 2.85 Å, Table 3). In jahnsite, there are two independent Fe octahedra alternating along the 7 Å axis. The Fe2 octahedra are located at the same level as the large *X* cation (Na^+ in jahnsite-(NaFeMg)) and they undergo similar small rotations as in segelerite, resulting in six Na–O distances in the range 2.43–2.57 Å and two longer distances of 2.82 Å (Kampf *et al.*, 2008). The Fe3 octahedra at the level of the small *M*1 cation (Fe^{3+} in jahnsite-[NaFeMg]), undergo much larger rotations of ~20°, in order to establish octahedral coordination around the small cation with six Fe–O distances in the range 1.98–2.09 in jahnsite-(NaFeMg) (Kampf *et al.*, 2008).

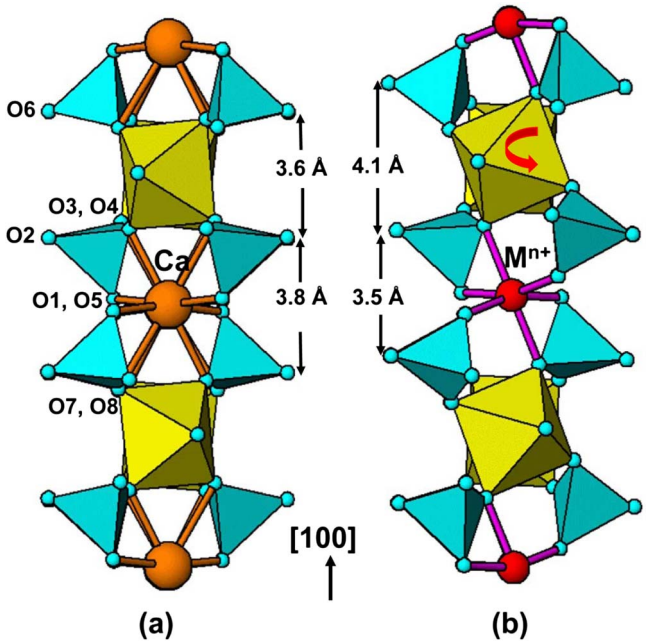

Fig. 6. Coordination of Ca in segelerite and of the small M^{n+} cation in jahnsite (= Fe^{3+} in jahnsite-[NaFeMg]). Projected separations along [100] are shown for the anions O2 and O6 that corner-link to Mg octahedra in both structures.

As shown in Fig. 6, the large octahedron rotations in jahnsite engender correspondingly large twistings of the PO_4 tetrahedra in the $Fe_2^{3+}(OH)_2(PO_4)_4$ columns, a consequence of which is significant changes to the positions of the anions O2 and O6 that connect to the Mg octahedra. This in turn requires that the Mg octahedra need to rotate about the 7 Å axis to maintain polyhedral connectivity. This rotation is much larger in jahnsite than in segelerite, as shown in Fig. 2, and it will influence the type of H-bonding that is possible. We suggest that the different magnitudes of the rotations of the Fe octahedra in segelerite and jahnsite in response to large- and small-cation ordering drives the symmetry changes in the two minerals so that a strong H-bonding network is maintained. It would be interesting to examine the situation where both *X* and *M*1 in jahnsite-group minerals are small cations. This situation occurs in jahnsite-(MnMnMn) and whiteite-(MnFeMg) (Moore & Ito, 1978) and in whiteite-(MnMnMg) (Elliott, 2016) but to date the crystal structures of these minerals have not been published.

Acknowledgements: Thanks to Colin MacRae for help with the EMP analyses. Barry Kayes kindly allowed access to the Mt Deverell variscite workings.

References

Bridge, P.J. & Pryce, M.W. (1974): Magnesian collinsite from Milgun Station, Western Australia. *Mineral. Mag.*, **39**, 577–579.

Capitelli, F., Chita, G., Cavallo, A., Bellatreccia, F., Della Ventura, G. (2011): Crystal chemistry of whiteite-(CaFeMg) from Crosscut Creek, Canada. *Z. Kristallogr.*, **226**, 731–738.

Elliott, P. (2016): Whiteite-(MnMnMg), IMA 2015–092. CNMNC Newsletter No. 29, February 2016, 202. *Mineral. Mag.*, **80**, 199–205.

Fetherston, J.M., Stocklmayer, S.M., Stocklmayer, V.C. (2013): Gemstones of Western Australia. Geological Survey of Western Australia. *Mineral Res. Bull.*, **25**, 306.

Gagné, O.C. & Hawthorne, F.C. (2015): Comprehensive derivation of bond-valence parameters for ion pairs involving oxygen. *Acta Crystallogr.*, **B71**, 562–578.

Gatta, G.D., Vignola, P., Meven, M. (2014): On the complex H-bonding network in paravauxite, $Fe^{2+}Al_2(PO_4)_2(OH)_2{\cdot}8H_2O$: A single crystal neutron diffraction study. *Mineral. Mag.*, **78**, 841–850.

Herwig, S. & Hawthorne, F.C. (2006): The topology of hydrogen bonding in brandite, collinsite and fairfieldite. *Can. Mineral.*, **44**, 1181–1196.

Kampf, A.R., Steele, I.M., Loomis, T.A. (2008): Jahnsite-(NaFeMg), a new mineral from the Tip Top mine, Custer County, South Dakota: Description and crystal structure. *Am. Mineral.*, **93**, 940–945.

Kampf, A.R., Adams, P.M., Nash, B.P. (2016): Whiteite-(CaMgMg), $CaMg_3Al_2(PO_4)_4(OH)_2{\cdot}8H_2O$, a new jahnsite-group mineral from the Northern Belle mine, Candelaria, Nevada, U.S.A. *Can. Mineral.*, **54**, 1513–1523.

Kampf, A.R., Alves, P., Kasatkin, A.Škoda, R. (2019): Jahnsite-(MnMnZn), a new jahnsite-group mineral, and formal approval of the jahnsite group. *Eur. J. Mineral.*, **31**, in press.

Larsen, E.S. III (1940): Overite and montgomeryite: two new minerals from Fairfield, Utah. *Am. Mineral.*, **25**, 315–326.

Moore, P.B. (1974): I. Jahnsite, segelerite and robertsite, three new transition metal phosphate species. II Redefinition of overite, an isotype of segelerite. III. Isotypy of robertsite, mitridatite and arseniosiderite. *Am. Mineral.*, **59**, 48–59.

Moore, P.B. & Araki, T. (1974): Jahnsite, $CaMn^{2+}Mg_2(H_2O)_8Fe_2^{3+}(OH)_2[PO_4]_4$: A novel stereoisomerism of ligands about octahedral corner-chains. *Am. Mineral.*, **59**, 964–973.

—,— (1977): Overite, segelerite and jahnsite: a study in combinatorial polymorphism. *Am. Mineral.*, **62**, 692–702.

Moore, P.B. & Ito, J. (1978): I. Whiteite, a new species, and a proposed nomenclature for the jahnsite-whiteite complex series, II. New data on xanthoxenite. III. Salmonsite discredited. *Mineral. Mag.*, **42**, 309–323.

Petříček, V., Dušek, M., Palatinus, L. (2014): Crystallographic computing system JANA2006: General features. *Z. Kristallogr.*, **229**, 345–352.

Sheldrick, G.M. (2015): Crystal structure refinement with *SHELXL*. *Acta Crystallogr.*, **C71**, 3–8.

Received 14 November 2018
Modified version received 6 December 2018
Accepted 18 December 2018